Nickel partitioning in biogenic and abiogenic ferrihydrite: The influence of silica and implications for ancient environments

Merle Eickhoff [a], Martin Obst [b], Christian Schröder [a,c,1], Adam P. Hitchcock [d], Tolek Tyliszczak [e], Raul E. Martinez [f], Leslie J. Robbins [g], Kurt O. Konhauser [g], Andreas Kappler [a,*]

[a] *Geomicrobiology, Center for Applied Geoscience, University of Tuebingen, Hoelderlinstraße 12, 72074 Tuebingen, Germany*
[b] *Environmental Analytical Microscopy, Center for Applied Geoscience, University of Tuebingen, Hoelderlinstraße 12, 72074 Tuebingen, Germany*
[c] *Environmental Mineralogy, Center for Applied Geoscience, University of Tuebingen, Hoelderlinstraße 12, 72074 Tuebingen, Germany*
[d] *Department of Chemistry and Chemical Biology, McMaster University, Hamilton, Ontario L8S 4M1, Canada*
[e] *Chemical Sciences Division, Lawrence Berkeley National Laboratory, Berkeley, CA 94720, USA*
[f] *Institut für Geo- und Umweltnaturwissenschaften, Albert-Ludwigs-Universität, Albertstraße 23b, 79104 Freiburg, Germany*
[g] *Department of Earth and Atmospheric Sciences, University of Alberta, Edmonton, Alberta T6G 2E3, Canada*

Abstract

Fe(III) (oxyhydr)oxides are ubiquitous in modern soils and sediments, and their large surface area leads to scavenging of trace elements. Experimental trace element partitioning between Fe(III) (oxyhydr)oxides and aqueous solutions have been used to elucidate the geochemical composition of the Precambrian oceans based on the trace element concentrations in Precambrian banded iron formations (BIFs). However, previous partitioning experiments did not consider the potential influence of microbially-derived organic material, even though it is widely believed that bacterial phytoplankton was involved in Fe(II) oxidation and the deposition of BIF primary minerals. Therefore, the present study focuses on sorption of Ni to, and co-precipitation of Ni with, both biogenic ferrihydrite precipitated by the freshwater photoferrotroph *Rhodobacter ferrooxidans* SW2 and the marine photoferrotroph *Rhodovulum iodosum*, as well as chemically synthesized ferrihydrite. We considered the influence of cellular organic material, medium composition and the availability of dissolved silica. Our results show a preferential association of Ni with ferrihydrite, and not with the microbial cells or extracellular organic substances. We found that the addition of silica (2 mM) did not influence Ni partitioning but led to the encrustation of some cells with ferrihydrite and amorphous silica. The two- to threefold lower Ni/Fe ratio in biogenic as compared to abiogenic ferrihydrite is probably due to a competition between Ni and organic matter for sorption sites on the mineral surface. Additionally, the competition of ions present at high concentrations in marine medium for sorption sites led to decreased Ni sorption or co-precipitation. Based on our data we conclude that, if the Fe(III) minerals deposited in BIFs were – at least to some extent – biological, then the Ni concentrations in the early ocean would have been higher than previously suggested. This study shows the importance of considering the presence of microbial biomass and seawater ions in paleomarine reconstructions.

* Corresponding author. Tel.: +49 7071 2974992; fax: +49 7071 295059.
  E-mail address: andreas.kappler@uni-tuebingen.de (A. Kappler).
[1] Now at: Biological and Environmental Sciences, School of Natural Sciences, University of Stirling, Stirling FK9 4LA, UK.

1. INTRODUCTION

Nickel (Ni) is incorporated into several specific Ni-dependent enzymes, such as NiFe-hydrogenases, carbon monoxide dehydrogenase, acetyl-CoA decarbonylase/synthase, methyl coenzyme M reductase and others (Mulrooney and Hausinger, 2003). Ni-enzymes are thought to have evolved early, as most of them are confined to anaerobic prokaryotes, such as methanogens, that were likely active on early Earth (e.g., Zerkle et al., 2005).

Estimates of trace metal bioavailability in Precambrian oceans may provide insights into the evolution of the biosphere based on the requirement of these metals by specific enzymes (e.g., Saito et al., 2003; Zerkle et al., 2005; Anbar, 2008; Robbins et al., 2013). The bioavailability of trace metals is tightly controlled by minerals such as Fe(III) (oxyhydr)oxides (Brown et al., 1998) due to their large reactive surface area and their high sorption affinity for metal cations (Cornell and Schwertmann, 2003). Recently it has been suggested that also green rust minerals, which form during abiotic or microbial Fe(II) oxidation and Fe(III) reduction (Parmar et al., 2001; Pantke et al., 2011; Zegeye et al., 2012) could similarly have been highly reactive iron substrates in the Precambrian oceans (Zegeye et al., 2012). Banded iron formations (BIFs) are major Fe-rich sedimentary deposits of the Precambrian. Because the primary Fe(III) (oxyhydr)oxides that initially formed BIF sediment scavenged trace elements such as Ni from the ocean waters at the time of their precipitation and deposition, they provide an archive of Precambrian ocean chemistry. In this regard, paleomarine reconstructions based on trace element partitioning experiments using abiotic Fe(III) (oxyhydr)oxides as proxies for primary BIF minerals have suggested a decline of oceanic Ni in the late Archean that might have limited methanogens, giving rise to the accumulation of atmospheric oxygen (Konhauser et al., 2009).

The Fe(III) (oxyhydr)oxides used for these previous studies were chemically synthesized. However, in modern environments Fe redox processes are mainly controlled by microbial Fe(II) oxidation and anaerobic Fe(III) reduction (Weber et al., 2006; Konhauser et al., 2011a). It is widely believed that anoxygenic phototrophic or microaerophilic Fe(II)-oxidizing bacteria were also involved in Fe(II) oxidation and the deposition of BIF primary minerals (e.g., Widdel et al., 1993; Konhauser et al., 2002; Kappler et al., 2005; Planavsky et al., 2009; Chi Fru et al., 2013; Posth et al., 2013b). It has been shown that biogenic Fe(III) (oxyhydr)oxides, consisting of cell–mineral aggregates, differ from abiogenic minerals by means of chemical composition, particle size and density (Posth et al., 2010), as well as surface properties (Ferris, 2005; Muehe et al., 2013). The formation of biogenic Fe(III) (oxyhydr)oxides is initiated by a biotic oxidation of Fe(II), and the following hydrolysis of Fe(III) and precipitation of primary minerals is inorganically driven and influenced by the chemical composition and available counter ions in the environment (Clarke et al., 1997; Konhauser et al., 1998; Larese-Casanova et al., 2010). This leads to differences between biogenic and abiogenic Fe(III) (oxyhydr)oxides that are caused by the microbial cells and microbially-derived organic compounds, such as extracellular polymeric substances (EPS), present in cell–mineral aggregates. Thus, despite plausible estimates of trace metal concentrations in the Precambrian ocean based on partitioning experiments with chemically synthesized Fe(III) (oxyhydr)oxides, it remains unclear whether microbial cells and organic compounds would have affected the partitioning of Ni and other trace metals. A potential biogenic origin of the primary minerals in BIFs could, therefore, require a re-interpretation of early ocean chemistry and the resultant evolution of the early biosphere.

In this study, biogenic Fe(III) minerals precipitated by the freshwater photoferrotroph *Rhodobacter ferrooxidans* strain SW2 and the marine photoferrotroph *Rhodovulum iodosum* were studied in comparison to abiogenic Fe(III) minerals with respect to their sorption and co-precipitation capacity for Ni. The spatial distribution of the sorbed and co-precipitated Ni in the cell–mineral aggregates was mapped and the influence of silica (Si) on Ni sorption and co-precipitation was determined, assuming that the Archean ocean was saturated with amorphous Si (e.g., Maliva et al., 2005; Konhauser et al., 2007). Finally, the implications of a potential biogenic origin of Precambrian Fe-rich sediments for Ni abundance in the Precambrian ocean are discussed.

2. EXPERIMENTAL PROCEDURES

2.1. Sources of the organisms

R. ferrooxidans strain SW2 was isolated from a freshwater mud sample from a pond in Schaumburger Wald, Hanover region, Germany (Ehrenreich and Widdel, 1994), and *R. iodosum* was isolated from a marine mud flat of the Jadebusen, North Sea, Germany (Straub et al., 1999). Both are Gram-negative purple non-sulfur bacteria belonging to the Alphaproteobacteria and grow photoautotrophically by oxidizing Fe(II) to Fe(III) or by using H_2 as electron donor.

2.2. Microbial growth media and growth conditions

All glassware used for biogenic and abiogenic experiments was soaked in 1 M HCl for 24 h and subsequently washed 6 times with MilliQ water to remove traces of metal ions. Both bacterial strains were cultivated in anoxic mineral medium with a reduced phosphate concentration of 0.5 mM. NaCl was added to compensate for the decrease in ionic strength due to the reduced phosphate concentration. The freshwater medium for strain SW2 contained 5.6 mM NH_4Cl, 0.5 mM KH_2PO_4, 5.6 mM NaCl, 0.68 mM $CaCl_2 \cdot 2H_2O$, and 2.0 mM $MgSO_4 \cdot 7H_2O$. The marine medium for *R. iodosum* contained 4.7 mM NH_4Cl, 0.5 mM KH_2PO_4, 10.2 mM $CaCl_2 \cdot 2H_2O$, 27.6 mM $MgSO_4 \cdot 7H_2O$, 28.0 mM $MgCl_2 \cdot 6H_2O$, 455.9 mM NaCl, 8.9 mM KCl, and 0.8 mM KBr. After autoclaving and cooling under N_2/CO_2 (90/10) gas, 22 mM bicarbonate buffer was added, which had been autoclaved under N_2/CO_2 atmosphere. Then the following solutions were added to the growth media from sterile stocks: 1 mL/L trace element solution SL 10 (Widdel et al., 1983), 1 mL/L vitamin solution

(Pfennig, 1978), 1 mL/L selenite–tungstate solution (Tschech and Pfennig, 1984). In addition 0.5 mM $N_2S_2O_3$ was added to the marine medium. The pH was adjusted to 7.0 for strain SW2 and to 6.8 for *R. iodosum*. The $FeCl_2$ was added to the medium from a sterile stock of anoxic 1 M $FeCl_2 \cdot 4H_2O$. Precipitated ferrous phosphate and ferrous carbonate were filtered out in an anoxic chamber using a 0.22 μm filter (polyethersulfone, Millipore), leaving approximately 2 mM of dissolved Fe(II) in solution and thus leading to a Fe(III) mineral concentration of 2 mM after oxidation. All cultures were inoculated from a pre-culture in Fe-free medium grown on H_2. Cultures were grown in 25 mL medium in 58 mL serum bottles at 20 °C and >600 lux under a tungsten light bulb until all Fe(II) was oxidized to Fe(III) (after 14 days in the absence of additional Si or Ni, after 14 days in the presence of 2 mM Si, after 14–28 days in the presence of 170 μM Ni and after 2 months in the presence of 2 mM Si and 170 μM Ni).

2.3. Abiogenic samples

Abiogenic ferrihydrite was synthesized by hydrolysis of $Fe(NO_3)_3 \cdot 9H_2O$ with KOH and subsequently the pH was adjusted to 7.0 as described by Cornell and Schwertmann (2003). The identity of the synthesized ferrihydrite was confirmed by Mössbauer spectroscopy. For sorption experiments, ferrihydrite with the simplified formula $Fe(OH)_3$ was diluted to a final concentration of 2 mM, while for co-precipitation experiments, the synthesis protocol was down-scaled so that only 2 mM ferrihydrite precipitated. This way, the same concentration of ferrihydrite was used for biogenic and abiogenic setups to allow for comparison. The ferrihydrite was synthesized and diluted in MilliQ water, as well as in the freshwater mineral medium as used for cultivation of strain SW2, or in the marine medium as used for *R. iodosum*. This was done to take into account the ions present in the medium when comparing the biogenic and abiogenic setups.

2.4. Experimental setup

The sorption and co-precipitation of Ni in the presence of biogenic and abiogenic ferrihydrite (2 mM) was determined at pH 6.8–7.0 (see Sections 2.2 and 2.3) in freshwater and marine medium. To a subset of samples, Si was added (2 mM) from a stock of anoxic 50 mM $Na_2O_3Si \cdot 9H_2O$ to mimic an early ocean saturated with amorphous Si and to examine the influence of Si on Ni sorption and co-precipitation. Si was added prior to inoculation and before microbial oxidation of Fe(II) or prior to abiotic ferrihydrite precipitation. Ni (170 μM) was added from a 1000 mg/L Ni ICP standard (in 2% HNO_3; Sigma Aldrich). For co-precipitation experiments, Ni was added before inoculation with the Fe(II)-oxidizing bacteria, or prior to abiotic precipitation of ferrihydrite. For sorption experiments, Ni was added after complete microbial oxidation of Fe(II) to Fe(III), or after precipitation of abiogenic ferrihydrite. The samples were equilibrated for 24 h in the dark on a rotary shaker. Duplicates of all cultures and abiotic samples were set up, in addition to one sterile control per biotic

setup. As a control for abiotic samples, medium without ferrihydrite was used.

2.5. Quantification of Fe, Si and Ni

Fe(II) and Fe(total) were quantified by the spectrophotometric ferrozine assay modified from Stookey (1970) and described by Hegler et al. (2008). Fe(II) and Fe(total) were quantified in all samples prior to inoculation and during microbial Fe(II) oxidation to determine the endpoint of Fe(II) oxidation in biotic samples, and of all abiotic ferrihydrite samples. Each sample was measured in triplicates. All biotic samples were taken in an anoxic chamber.

The concentration of dissolved Si was determined with the spectrophotometric molybdosilicate method (Eaton et al., 2005). Each sample was measured in triplicates.

The amount of sorbed or co-precipitated Ni was determined by subtracting the final Ni concentration in solution after sorption or co-precipitation from the initial Ni concentration. All Ni concentrations were determined by ICP-OES. In co-precipitation experiments, Ni was added to a final concentration of 10 mg/L (170 μM) to each sample prior to inoculation of the sample with bacteria for biotic samples, and before precipitation of ferrihydrite in abiotic samples. After complete oxidation of Fe(II) to Fe(III) or abiotic ferrihydrite precipitation, samples for quantification of final Ni concentrations were filtered using a 0.22 μm nylon filter (Costar, Corning, NY). Aliquots of 990 μL were taken from the filtrate and acidified with 10 μL conc. HNO_3.

In sorption experiments, Ni was added to a final concentration of 10 mg/L (170 μM) to each sample after complete oxidation of Fe(II) to Fe(III) or after precipitation of ferrihydrite in abiotic samples. After 24 h equilibration on a rotary shaker in the dark, samples for quantification of final Ni concentrations were taken and filtered using a 0.22 μm nylon filter (Costar, Corning, NY) in an anoxic chamber. Aliquots of 990 μL were taken from the filtrate and acidified with 10 μL conc. HNO_3.

Samples were then diluted 1:10 in MilliQ water and acidified with concentrated HNO_3 to 1.5% HNO_3. Ni was quantified at a wavelength of 231.604 nm by ICP-OES with a Perkin Elmer Optima 5300 DV equipped with a Meinhard Nebulizer Cyclonic Spray Chamber (non-baffled) for analyses in freshwater medium, and with a Mira Mist Nebulizer for analyses in marine medium. For each setup, two separate samples and a control (see Section 2.4) were measured. Standards for calibration contained the respective medium with a dilution factor of 1:10 as the matrix.

2.6. Mineral characterization

Mössbauer spectroscopy was performed as described previously (Larese-Casanova et al., 2010). In an anoxic glove box, the samples were filtered onto 0.45 μm membranes (mixed cellulose esters) and the minerals preserved between two layers of oxygen-impermeable Kapton tape (Polyfluor Plastics BV, The Netherlands). ^{57}Fe Mössbauer spectroscopy was performed with a ^{57}Co source at room temperature with linear acceleration in transmission mode.

The sample temperature was varied using a Janis closed-cycle cryostat with a helium atmosphere. Spectra were calibrated against spectra of α-Fe(0) foil at room temperature and interpreted using Recoil software (University of Ottawa, Canada) and Voigt-based fitting models. For each setup, one sample was analyzed. Estimated errors are ±0.02 mm/s for isomer shift (IS) and quadrupole splitting (QS) values, and ±1 T for hyperfine magnetic field (B_{hf}) values.

For specific surface area (SSA) analysis, the abiogenic minerals, biogenic cell–mineral aggregates or bacterial cells grown with H_2 were harvested by centrifugation at $4000g$ and freeze-dried. The SSA of the particles was measured using N_2 adsorption by Brunauer–Emmett–Teller (BET) analysis with an ASAP 2000 (Micromeritics) at 77 K after degassing under vacuum for 15–20 h at 40 °C. For each setup, one sample was analyzed.

2.7. Scanning transmission X-ray microscopy (STXM)

Samples for STXM were taken after complete oxidation of Fe(II) to Fe(III). Therefore, the samples were not sensitive to oxygen and could be processed under oxic conditions. 1 mL of the culture or abiogenic mineral suspension was sampled and washed carefully twice in Millipore water to eliminate salts and non-sorbed Ni from solution. For samples not containing Si, 1 µL of the resuspended pellet was applied to a silicon nitride window (Norcada Inc., Edmonton, Canada) and air-dried before the window was fixed to an aluminum sample holder. For samples containing Si, a formvar coated 300 mesh Cu transmission electron microscopy (TEM) grid was immersed into the resuspended pellet, air-dried and then fixed to the sample holder.

Most STXM experiments (data shown in Fig. 4a–n and Fig. 5a–h) were carried out at the spectromicroscopy beamline 10ID-1 at the Canadian Light Source (CLS, Saskatoon, Canada), which is described in more detail by Kaznatcheev et al. (2007). Image stack-maps were acquired across the C-1s, O-1s, Fe-2p and Ni-2p edges, and full image sequences (stacks) were acquired across the C-1s and Fe-2p edges with a spectral sampling of 0.1 eV in the energy regions of interest (Hitchcock et al., 2009; Miot et al., 2009a; Table S1). For the mapping of Si, some additional experiments (data shown in Fig. 5i–q) were carried out at the STXM beamline 11.0.2 at the Advanced Light Source (ALS, Berkeley, CA, USA), which is described in more detail by Bluhm et al. (2006). Here, image stack-maps and image stacks were acquired across the O-1s, Fe-2p, Ni-2p and Si-1s edges with spectral samplings of 0.1 eV (O-1s and Fe-2p) and 0.6 eV (Si-1s) in the energy regions of interest.

The program aXis2000 (Hitchcock, 2013) was used to create quantitative elemental maps. Image sequences were converted from transmission to linear absorbance (optical density, OD; Dynes et al., 2006). Quantitative mapping was done as described previously (Dynes et al., 2006; Hitchcock et al., 2009) by one of three different ways: (i) image difference maps display the difference between two images, one measured at the main absorption peak of the chemical species of interest, the other measured in the pre-edge at an energy below the absorption onset of that species (refer to Table S1 for the energies used). (ii) To reduce statistical noise in image difference maps, the difference between the average of five images measured at the absorption peak and the average of five images measured in the pre-edge is displayed. (iii) In the third, most precise way, image sequences (stacks) at various energies across the desired absorption edge were fitted quantitatively using spectra of known reference compounds, and the optical density converted to effective thickness in nm. Quantification of Ni/Fe was based on the average OD of Ni and Fe in the same region of interest. For quantification, the Ni and Fe maps were threshold-masked to separate absorption signal from statistical noise.

3. RESULTS

3.1. Mineral identification and characterization

Before quantification of Ni partitioning in biogenic and abiogenic Fe(III) minerals, we determined their mineralogy, composition and structure. Both biogenic and abiogenic Fe(III) minerals were identified using Mössbauer spectroscopy. The mean magnetic hyperfine field (B_{hf}), the quadrupole splitting and the isomer shift measured at different temperatures, identified all biogenic and abiogenic samples precipitated in freshwater or marine medium as ferrihydrite (Fig. S1; Tables S2 and S3). However, an influence on the mineralogy arising from the ions present in the medium was observed, as the B_{hf} of 45.6–46.1 T measured at 4.2 K was lower for ferrihydrite precipitated in marine medium (ionic strength of 0.72 M) as compared to those precipitated in freshwater medium (ionic strength of 0.04 M; Fig. 1) with a B_{hf} of 47.4–48.0 T. This effect was also observed for samples precipitated in the presence of additional Si prior to ferrihydrite precipitation. This resulted
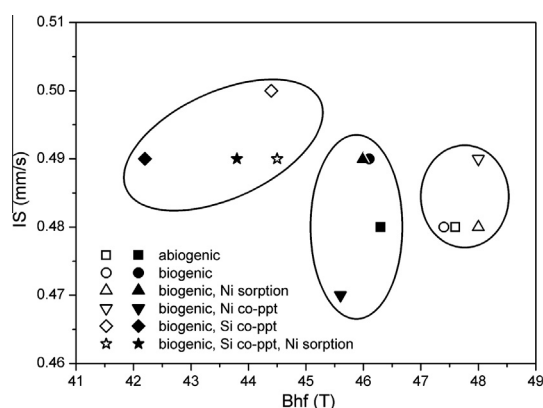

Fig. 1. Mössbauer spectroscopy analyses of biogenic and abiogenic Fe(III) (oxyhydr)oxides showing the isomer shift (IS) relative to the mean magnetic hyperfine field (B_{hf}) at 5 K. The B_{hf} at 5 K is dependent on the medium in which biogenic or abiogenic ferrihydrite was precipitated and on the presence or absence of additional silica. The right circle contains freshwater samples with the highest B_{hf}, the middle circle contains marine samples with a lower B_{hf}, and the left circle contains freshwater and marine samples precipitated in the presence of additional Si with the lowest B_{hf}. Open symbols: ferrihydrite precipitation in freshwater medium; solid symbols: ferrihydrite precipitation in marine medium.

in an even lower B_{hf} of 44.4–44.5 T for freshwater and 42.2–43.8 T for marine samples (Fig. 1). Ni sorption or co-precipitation did not influence the B_{hf}.

The effects of Ni and Si on the mineralogy became more apparent in measurements at 77 K. The magnetic ordering temperature in ferrihydrite generally increases with greater crystallinity and/or particle size, i.e., with the transition from 2-line ferrihydrite to 6-line ferrihydrite. The abiogenic 2-line ferrihydrite synthesized in freshwater medium did not show any magnetic ordering at 77 K (Fig. 2a and b) and was used for comparison to biogenic minerals. Biogenic minerals precipitated by *R. ferrooxidans* SW2 in freshwater medium showed the onset of magnetic ordering at 77 K in the absence of Si (Fig. 2c; Table S3), while the presence of Si seemed to

prevent this (Fig. 2d; Table S3). A larger extent of magnetic ordering was visible in spectra of ferrihydrite measured at 77 K with sorbed or co-precipitated Ni (Fig. 2e and g; Table S3), while this magnetic ordering effect was also not observed in the presence of Si (Fig. 2f; Table S3).

Interestingly, after sorption of Ni to biogenic ferrihydrite in freshwater medium, 4% and 3% of Fe(II) was detected in the Mössbauer spectra in the absence (Fig. 2e) and presence (Fig. 2f) of Si, respectively (Table S3). The Fe(II) must have formed during the time of incubation with Ni to the time of sample preparation for Mössbauer spectroscopy (20 days), because Ni was added to the cultures only after all Fe(II) had been oxidized to Fe(III), as determined by the ferrozine assay. Fe(II) was not detected for Ni co-precipitation in the
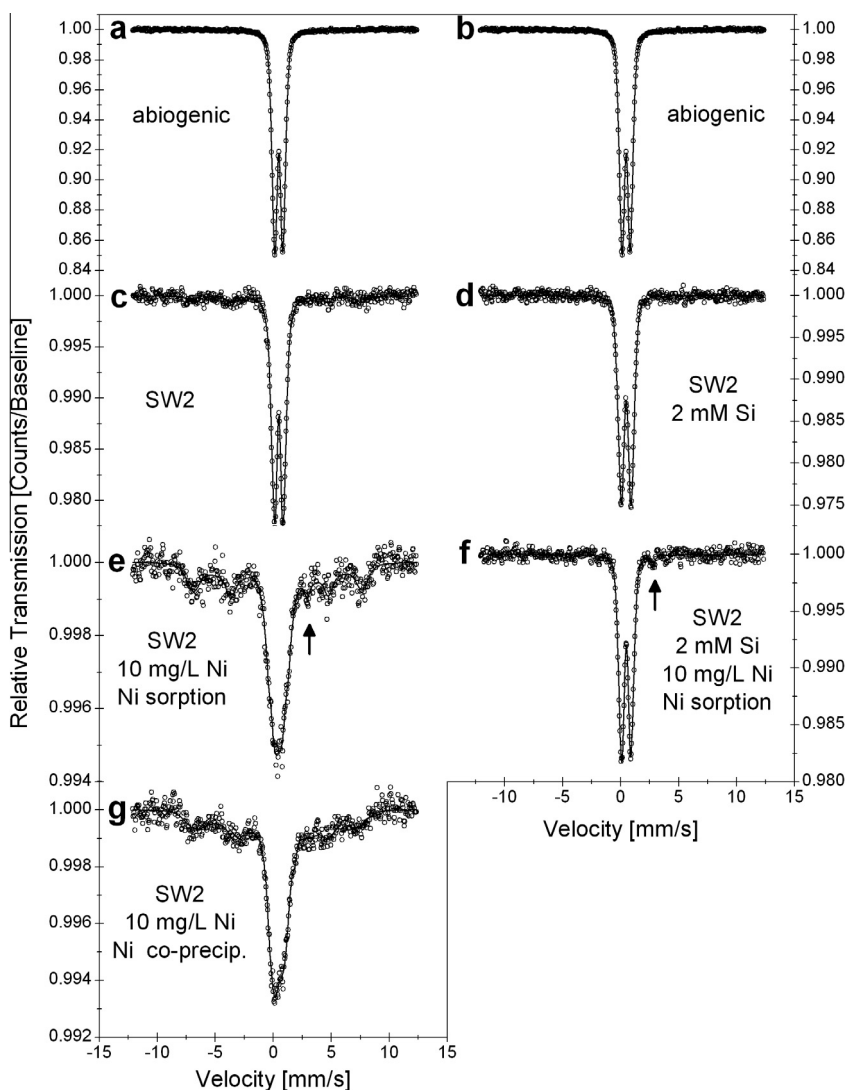

Fig. 2. Mössbauer spectra, recorded at 77 K, of biogenic and abiogenic ferrihydrite precipitated in freshwater medium. Abiogenic ferrihydrite (a, b) was precipitated by hydrolysis of $Fe(NO_3)_3 \cdot 9H_2O$ with KOH in freshwater medium. Spectra of biogenic ferrihydrite are shown for precipitation in the absence (left c, e, g) and presence (right d, f) of 2 mM Si. Biogenic ferrihydrite was precipitated by oxidation of Fe(II) by the photoferrotroph *Rhodobacter ferrooxidans* SW2 in freshwater medium without addition of Ni in the absence (c) and in the presence of Si (d). After sorption of 10 mg/L (170 μM) Ni to biogenic ferrihydrite, Fe(II) was detected in the spectra (black arrow) in the absence (e) and presence (f) of Si, but was not detected after co-precipitation of Ni with biogenic ferrihydrite (g). For all biogenic samples precipitated in the absence of Si (c, e, g), an increased magnetic order of ferrihydrite is visible, which is absent from samples precipitated in the presence of Si (d, f) or from abiogenic samples (a, b). Open circles show the measured data, the solid line represents an overall fit.

freshwater medium (Fig. 2g) or biogenic ferrihydrite precipitated in the marine medium (Fig. S2; Table S3). The formation of Fe(II) will have to be investigated further as this is not the focus of the present study.

The quadrupole splitting recorded at room temperature (Table S2) increased from 0.76 to 0.86 mm/s for biogenic freshwater and from 0.75 to 0.85 mm/s for biogenic marine minerals precipitated in the presence of Si when compared to biogenic minerals formed in the absence of Si.

The specific surface area (SSA) of biogenic ferrihydrite was roughly 2 or 3 times smaller (100 and 130 m^2/g) than that of abiogenic ferrihydrite (270 and 220 m^2/g) in freshwater or marine medium, respectively (Table 1). The SSA of abiogenic ferrihydrite precipitated in either freshwater or marine medium was in the same range as that for ferrihydrite precipitated in MilliQ water with a value of 280 m^2/g. Bacterial cells grown with H_2 and in the absence of minerals exhibited only a low N_2-BET SSA of approximately 1 m^2/g (Table 1).

3.2. Quantification of Ni sorption and co-precipitation with biogenic versus abiogenic ferrihydrite

After identification of all Fe(III) minerals, Ni sorption to, and co-precipitation with, biogenic and abiogenic ferrihydrite were quantified by ICP-OES by measuring Ni concentrations in solution after Ni partitioning (Table S4). Solid-free control samples showed no loss of Ni to the glass containers. Co-precipitation of Ni led to a higher Ni content in ferrihydrite than sorption in all cases (Fig. 3a). More precisely, Ni co-precipitation with biogenic ferrihydrite in freshwater or marine medium resulted in molar Ni/Fe ratios of 0.032 and 0.017, respectively, and was roughly 3 or 2 times higher than Ni sorption to biogenic ferrihydrite in freshwater and marine samples with molar Ni/Fe ratios of 0.010 and 0.007, respectively (Fig. 3a). Ni co-precipitation with abiogenic ferrihydrite in freshwater medium with a molar Ni/Fe ratio of 0.061 was also 3 times higher than Ni sorption to abiogenic ferrihydrite with a molar Ni/Fe ratio of 0.019. Ni co-precipitation with abiogenic ferrihydrite in marine medium was not determined. Moreover, Ni

co-precipitation with, and Ni sorption to, biogenic ferrihydrite in freshwater medium were increased by factors of 2 and 1.4, respectively, compared to Ni co-precipitation with, and sorption to, biogenic ferrihydrite in marine medium. Showing the same trend, the Ni/Fe ratio of 0.019 for Ni sorption to abiogenic ferrihydrite in freshwater medium was 1.7 times higher than in marine medium with a Ni/Fe ratio of 0.011 (Fig. 3a). In addition, Ni sorption and co-precipitation with abiogenic ferrihydrite showed higher values than with biogenic ferrihydrite for both freshwater and marine setups. Specifically, Ni sorption to abiogenic ferrihydrite in freshwater or marine medium was increased by factors 1.8 or 1.5, respectively, compared to biogenic ferrihydrite, while Ni co-precipitation with abiogenic ferrihydrite in freshwater medium was higher than with biogenic ferrihydrite by a factor of 2 (Fig. 3a).

The influence of Si on sorption and co-precipitation of Ni with ferrihydrite was also determined. All trends observed in the absence of Si were confirmed in samples in which Si was present before the precipitation of ferrihydrite, i.e., Ni co-precipitation was higher than Ni sorption (by factors of 4 and 5) for biogenic freshwater and marine samples, respectively. In freshwater medium, sorption and co-precipitation of Ni was higher than in marine medium, and Ni sorption and co-precipitation with abiogenic was higher than with biogenic ferrihydrite (Fig. 3b). Si did not show a significant influence on the amount of Ni sorbed or co-precipitated with ferrihydrite for the chosen concentrations of Fe and Si (see below). In the case of biogenic ferrihydrite in marine medium, the Ni/Fe ratio for Ni sorption decreased by a factor of 2 in the presence of Si, and in the case of Ni co-precipitation with biogenic ferrihydrite in freshwater medium, the presence of Si increased the Ni/Fe ratio by a factor of 1.3. In all other cases, the influence of Si was minor or absent (Fig. 3b).

3.3. Spatial distribution of Fe, Ni, Si and protein

STXM was applied to determine the elemental/chemical distribution in the samples. A comparison of the Fe, Ni and protein maps of the biogenic samples with Ni sorption in freshwater and marine medium (Fig. 4a–c and e–g), as well as the illustration in the overlays (Fig. 4d and h), reveals that Ni is associated preferably with ferrihydrite and not with cells (using the protein signal as a proxy for cells). In samples where Ni was sorbed to abiogenic ferrihydrite in freshwater and marine medium, Ni was clearly associated with the minerals (Fig. 4i, k and l, m). For a quantitative evaluation of the image maps, data for Ni co-precipitation were also included (images for Ni co-precipitation not shown). Quantification was based on the average ODs of Fe and Ni in the same region of interest and showed that Ni/Fe ratios for Ni co-precipitation were higher than those for Ni sorption in all cases, that Ni/Fe ratios for all freshwater samples were higher than those for marine samples in both biogenic and abiogenic setups, and that Ni/Fe ratios for abiogenic ferrihydrite were higher than those for biogenic ferrihydrite in both freshwater and marine medium (Fig. 4n). This trend on the microscopic scale is in good agreement with the data obtained by ICP-OES (Fig. 3a).

Table 1
Specific surface areas of abiogenic and biogenic ferrihydrite synthesized in different media, and of bacterial cells without minerals.

Mineral	SSA[a] (m^2/g)
Biogenic Fh[b] in FM[c] (SW2)	100
Abiogenic Fh[b] in FM[c]	270
Biogenic Fh[b] in MM[d] (R. iodosum)	130
Abiogenic Fh[b] in MM[d]	220
Abiogenic Fh[b] in MQ[e]	280
Bacterial cells (SW2)	~1[f]

[a] Specific surface area; one sample measured per setup.
[b] Ferrihydrite.
[c] Freshwater medium.
[d] Marine medium.
[e] Milli-Q water.
[f] SSA approximately 1 m^2/g but it has to be noted that sample degassing was incomplete indicated by slightly higher N_2-desorption than sorption values. This suggests that the true SSA of dried bacterial cells is probably slightly higher than 1 m^2/g.
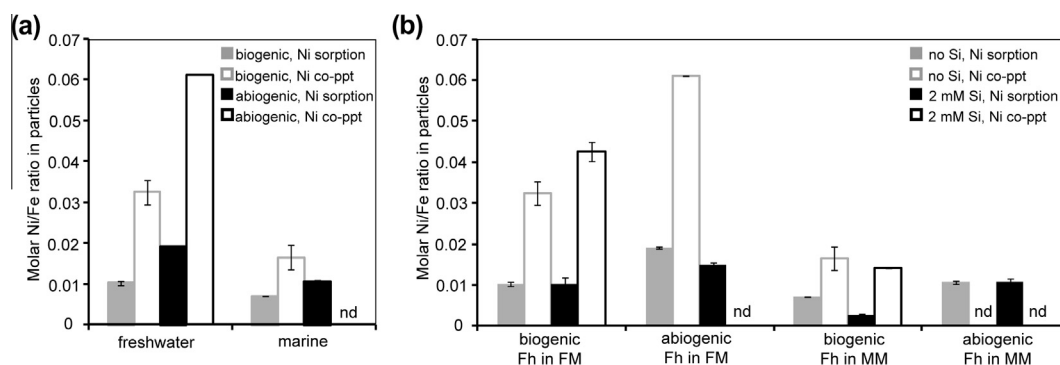
Fig. 3. Quantification of Ni sorption to, and co-precipitation (co-ppt) with ferrihydrite. Aqueous (non-sorbed) Ni was quantified by ICP-OES. (a) Ni sorption to and co-precipitation with biogenic and abiogenic ferrihydrite in both freshwater and marine setups. (b) Ni sorption to and co-precipitation with biogenic and abiogenic ferrihydrite in freshwater and marine setups in the presence and absence of silica. Error bars indicate the range of values of two independent samples. Where no error bar is present, only one sample was analyzed. Fh, ferrihydrite (abiogenic Fh was precipitated by hydrolysis of $Fe(NO_3)_3 \cdot 9H_2O$ by KOH); FM, freshwater medium; MM, marine medium.

However, the values themselves should not be directly compared because they were based on OD-ratios for STXM and on molar ratios for ICP-OES analyses.

In the presence of Si, only biogenic samples with ferrihydrite precipitated by *R. ferrooxidans* SW2 in freshwater medium were analyzed by STXM. Comparing Fe and protein maps shows that in the presence of Si, Fe was directly associated with the cells in a few cases (Fig. 5a, c and e, g). This phenomenon was observed in two separate cultures analyzed (samples shown in Fig. 5a–d stemming from one culture, samples shown in Fig. 5e–h stemming from a separate culture) in the presence of Si, while co-localization of cells and Fe was not observed in samples which did not contain Si (Fig. 4a, c and e, g). Energies at the CLS did not allow the mapping of Si directly. However, a high absorption in the C-1s pre-edge at 280.0 eV (Fig. 5d) suggests that Si causes this absorption because Si was the only other abundant element in the medium, and its Si-2p absorption edges at ∼100 eV (Bearden and Burr, 1967) are in the C-1s pre-edge. Ni in these samples was co-located with Fe, and where Fe was associated with protein, Ni was co-located with protein as well. However, it should be noted that these cells did not represent the bulk of the samples. Due to the limited available beamtime, we were unable to analyze all sample spots in detail, and had to prioritize the analysis of certain regions of interest based on a coarse sample screening. These Fe-associated cells represented noticeable exceptions. For a better understanding of the influence of Si, another sample was analyzed at a subsequent shift of beamtime at beamline 11.0.2 at the ALS. In this case, a coarse scan of this sample did not find cells associated with Fe, but Si clearly co-located with Fe in this sample (Fig. 5i, l and n, p) and not with protein, which is nicely demonstrated by the overlays in Fig. 5m and q.

4. DISCUSSION

4.1. Mineralogy of biogenic and abiogenic Fe(III) minerals

In this study, sorption of Ni to, and co-precipitation of Ni with, both abiogenic Fe(III) minerals and biogenic Fe(III) minerals, i.e., cell–Fe(III) mineral aggregates, were investigated. All biogenic and abiogenic Fe(III) minerals were identified as ferrihydrite by Mössbauer spectroscopy, regardless of the medium that they were precipitated in (freshwater or marine) and independent of the presence of Ni and Si. Previous findings of the formation of goethite by strain SW2 (Kappler and Newman, 2004; Posth et al., 2010) could not be confirmed in the present study. *R. iodosum* has been shown before to precipitate mostly ferrihydrite in unfiltered medium, with traces of magnetite (Straub et al., 1999).

Despite all minerals being identified as ferrihydrite, an influence of the media solution chemistry on the ferrihydrite structure and crystallinity was observed. The B_{hf} values in the 5 K spectra of ferrihydrite precipitated in marine medium (Table S2) are generally lower than those reported for ferrihydrite prepared in the laboratory (B_{hf} between 47 and 50 T; Murad and Cashion, 2004). However, they are comparable to those reported from natural samples recovered from marine environments (Chakarova et al., 2013). A decrease of B_{hf} values can be a result of (a) substitution of Fe by other cations or vacancies, or (b) a decrease in particle size. Cations or vacancies substituting for Fe have a magnetic moment that is different from that of Fe or no magnetic moment at all. As a result, the magnetic ordering temperature is generally lowered and the resulting internal magnetic field B_{hf} decreases. Substitution also distorts the crystal structure, as the substituting ions have a different radius and/or valence state, which needs to be balanced by vacancies elsewhere. The QS parameter in spectra above the magnetic ordering temperature, i.e., where sextets in the Mössbauer spectra have collapsed to doublets, is a measure of structural symmetry. It should increase upon substitutions that alter the structure (e.g. Rancourt et al., 2001; Eusterhues et al., 2008). By contrast, sorption of elements or ligands to the surface of ferrihydrite, even if occluded, does not alter the crystal structure and therefore does not lead to any changes in the Mössbauer parameters.

Particle size can affect B_{hf} values when the particles become smaller than approximately 30 nm. The particles then show superparamagnetic behavior, i.e. the magnetic domain sizes are comparable to particle sizes and are flipped randomly through thermal activity of the particles,
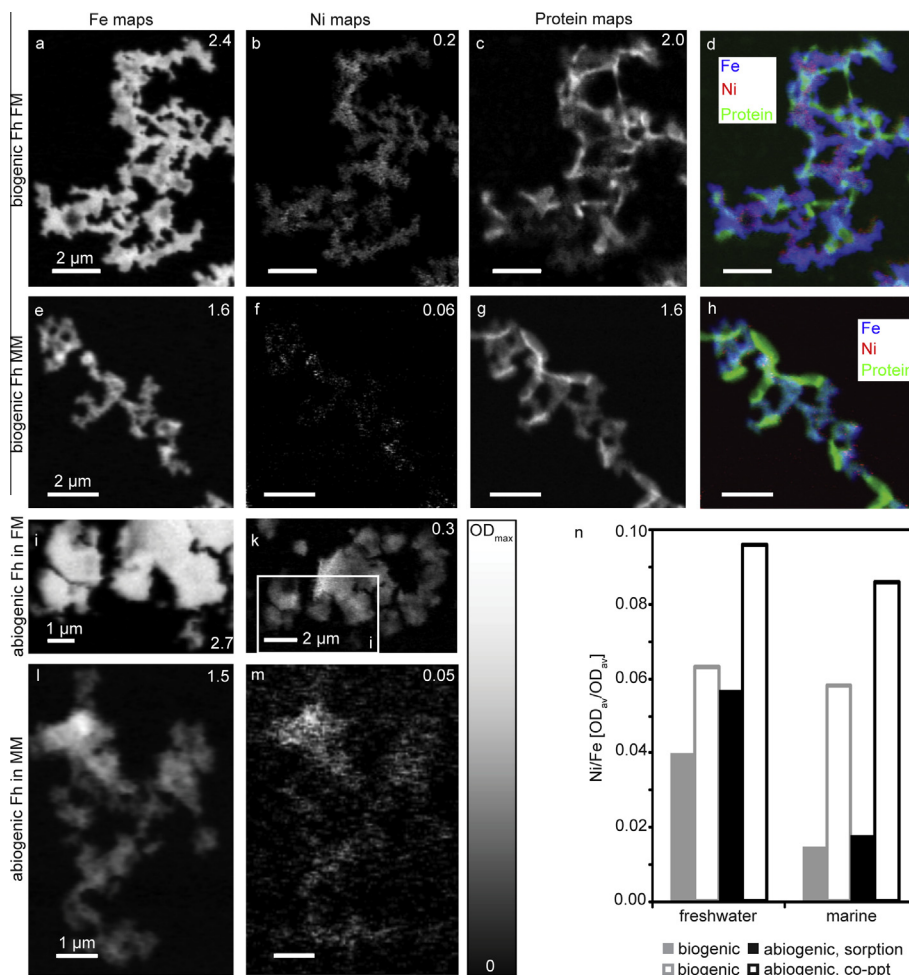
Fig. 4. Scanning transmission X-ray microscopy optical density (OD) maps and a quantitative evaluation of Ni sorbed to biogenic cell–mineral aggregates and abiogenic ferrihydrite. Fe (a, e, i, l) and Ni (b, f, k, m) image difference maps were obtained for biogenic and abiogenic setups, protein image difference maps (c, g) measured at the C-1s edge were additionally obtained from biogenic samples (see Table S1 for energies used). The white rectangle in (k) indicates the equivalent subarea analyzed in more detail at the Fe-2p edge, shown in (i). The gray scales indicate OD with the maximal OD given for each image. The scale bars are the same for one row of images if not indicated otherwise. Overlay images (d, h) demonstrate the spatial distribution of Fe, Ni and protein in the respective sample. The quantitative evaluation (n) shows the Ni/Fe ratio based on average ODs extracted from each image and reveals the sorption and co-precipitation (co-ppt) of Ni to biogenic and abiogenic ferrihydrite precipitated in freshwater and marine medium (images for Ni co-precipitation and for marine samples not shown). All images were obtained at the CLS. Fh, ferrihydrite; FM, freshwater medium; MM, marine medium.

which results in a net zero magnetic field. Magnetic ordering can be restored by lowering the temperature, and this so-called blocking temperature decreases as the average particle sizes become smaller. In the case of very small particles it may be that the blocking temperature is close to 5 K, in which case full magnetic ordering is not yet restored at 5 K, resulting in the observation of decreased B_{hf}.

We generally observe lower B_{hf} values in the marine medium samples compared to the freshwater medium samples. Excluding the Si-coprecipitation experiments, we do not observe an increase in QS values in the 77 K or RT spectra. Surface areas derived from BET measurements (Table 1) are not generally smaller for ferrihydrite precipitated in marine medium. We conclude from these observations that ferrihydrite precipitated in the marine medium had substitutions of Fe by other elements but with minimal

structural change. That requires substitution of Fe^{3+} by other ions of the same valency, for example Al^{3+}. Different bacterial strains do not influence the ferrihydrite crystal structure as we do not observe any significant differences in the Mössbauer parameters between biogenic and abiogenic ferrihydrite precipitated in the same medium.

In spectra from the Si-coprecipitation experiments we observe a further and very significant decrease in B_{hf} values in marine medium, a similar significant decrease in B_{hf} values in freshwater medium, and a significant increase in QS values in both marine and freshwater media. We therefore conclude that some Fe^{3+} has been substituted by Si^{4+} in these experiments. In addition, we do not observe any difference in the Mössbauer parameters between experiments in the presence or the absence of Ni, nor do we observe any significant differences between Ni sorption and Ni
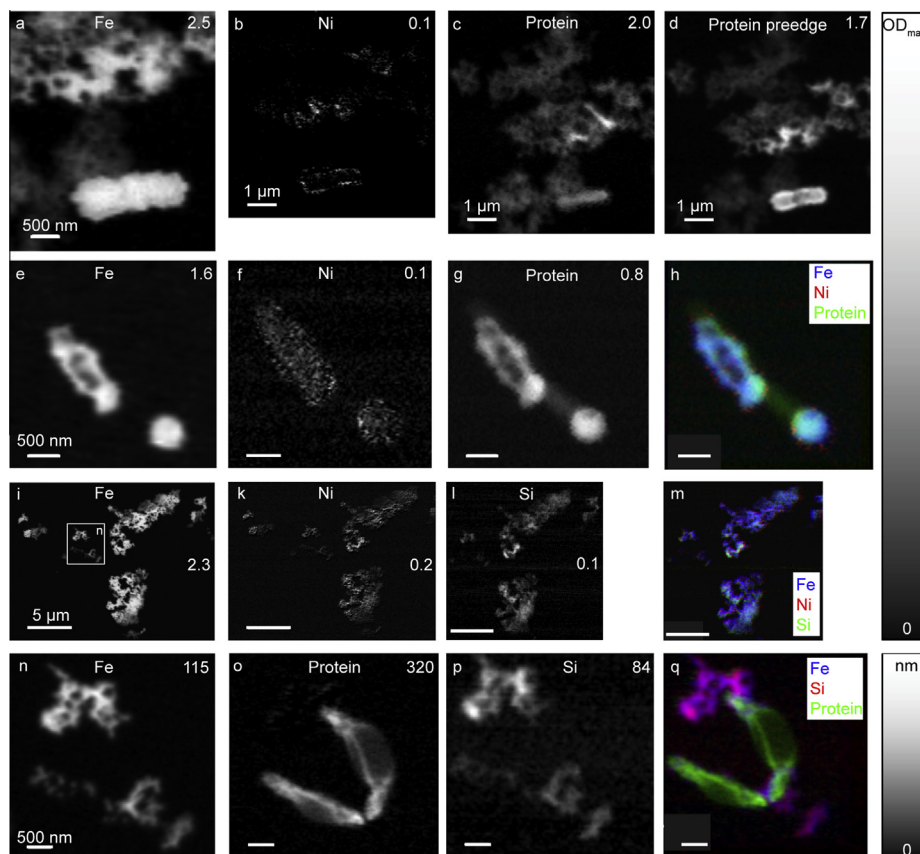
Fig. 5. Scanning transmission X-ray microscopy maps of samples of Ni sorption to biogenic ferrihydrite precipitated by the photoferrotroph *Rhodobacter ferrooxidans* SW2 in freshwater medium in the presence of Si. Data for images a-h were obtained at the CLS, data for images i-q at the ALS. Fe (a, e, i), Ni (b, f, k), protein (c, g) and Si (l) image difference maps are shown (see Table S1 for energies used). The protein image difference map in c was obtained at the C-1s edge, image d shows absorption in the C-1s pre-edge. Protein image difference map in g was obtained at the O-1s edge. The gray scales of (a–g) and (i–l) indicate OD with the maximal OD given for each image. The white rectangle in (i) indicates the subarea analyzed again in higher magnification and shown in (n–p). This area was analyzed by spectral fitting of recorded image sequences over the respective absorption peak using spectra of reference compounds (Table S1). The gray scales for these images (n–p) indicate effective thickness in nm with the maximal thickness given for each image. Overlay images (h, m, q) demonstrate the spatial distribution of Fe, Ni and Si or protein in the respective sample. The scale bars are the same for one row of images if not indicated otherwise.

coprecipitation experiments. This further suggests that Ni sorbs to ferrihydrite surfaces and might be occluded but is not incorporated into the crystal structure.

We also observed the onset of magnetic ordering, i.e. the emergence of sextets, in 77 K spectra of biogenic ferrihydrite precipitated by SW2 in freshwater medium. This implies that, compared to the abiogenic ferrihydrite, the biogenic ferrihydrite has slightly higher crystallinity or particle size. The medium composition can be excluded as the determining factor because in that case the abiogenic ferrihydrite synthesized in freshwater medium should have also shown an increased magnetic ordering, but this was not the case.

The fact that increased magnetic order was not detected at 77 K for biogenic ferrihydrite precipitated in marine medium by *R. iodosum* also rules out microbially-derived organic compounds or cells as the cause for an increased magnetic order; in particular since organic substances are typically known to decrease the magnetic order of ferrihydrite (Schwertmann et al., 2005; Mikutta et al., 2008). However, the rate and mechanism of ferrihydrite precipitation

can probably explain the increased magnetic order at 77 K of biogenic ferrihydrite precipitated by the freshwater strain SW2. While abiogenic ferrihydrite was formed by rapid hydrolysis of $Fe(NO_3)_3 \cdot 9H_2O$ with KOH within minutes, the biogenic ferrihydrite was produced by slow microbial oxidation of Fe(II) over a time span of at least 14 days. This slow formation of ferrihydrite allows more time for slow crystal formation and may lead to a slightly more crystalline structure as indicated by the increased magnetic order (Cornell and Schwertmann, 2003). However, in the environment, ageing of minerals may equalize crystallinity of both mineral synthesis routes on a time scale relevant for sedimentation and mineral deposition. This would leave the slightly higher crystallinity of biogenic ferrihydrite observed under laboratory conditions with only minor importance for an ancient ocean scenario. Moreover, the high concentrations of seawater ions of the marine medium seemed to interfere with crystal formation and prevent an increased magnetic order at 77 K in biogenic and abiogenic ferrihydrite. Also in the presence of Si, an increased magnetic order was not observed at 77 K. Si is known to form

strong and stable complexes on ferrihydrite surfaces, thereby interfering with crystal formation and crystal growth (e.g., Doelsch et al., 2000; Pokrovski et al., 2003; Cismasu et al., 2011). Indeed, the effect of Si interfering with crystal formation in our study could be inferred from the increased quadrupole splitting.

The specific surface area (SSA) of the minerals was determined by BET measurements to estimate the available surface area for Ni sorption. We found that the medium in which the ferrihydrite was precipitated did not influence the SSA significantly. The lower SSA of biogenic ($100–130 \ m^2/g$) as compared to abiogenic ferrihydrite ($220–270 \ m^2/g$) is in agreement with the higher crystallinity of biogenic ferrihydrite synthesized in freshwater medium as observed by Mössbauer spectroscopy. However, it has to be kept in mind that BET sample preparation could have changed the particles and available surface area. The vacuum drying and degassing might lead to (partial) blocking of the ferrihydrite surface and micropores by microbially-derived organic substances or whole cells which themselves exhibit a negligibly low N_2-BET SSA ($\sim 1 \ m^2/g$). As a consequence, this suggests a smaller mineral surface than what actually exists under wet conditions.

4.2. Ni sorption and co-precipitation with biogenic versus abiogenic ferrihydrite

Ni partitioning in biogenic and abiogenic ferrihydrite was determined by quantifying dissolved Ni concentrations after sorption or co-precipitation. A total Ni concentration of 10 mg/L (170 µM) was chosen based on previous experiments that showed that such concentrations are necessary for successful detection with STXM (Hitchcock et al., 2009). It should be noted that this concentration is vastly in excess of natural marine waters where Ni concentrations are around 9 nM, and even higher than estimated Archean seawater concentrations of 400 nM (Konhauser et al., 2009).

We found that Ni co-precipitation with ferrihydrite was roughly 2–3 times higher than Ni sorption in all setups. This is probably due to the fact that in the Ni sorption experiments Ni can bind only to the mineral surface sites that are available after complete oxidation of Fe(II) and Fe(III) mineral precipitation. In contrast, Ni co-precipitation includes Ni sorption to constantly forming new surface sites and occlusion by the forming crystals during precipitation, thereby removing more Ni from solution than sorption. An incorporation of Ni ions into the crystal lattice of hydrous ferric oxide (HFO) has not been observed (Xu et al., 2007). The high ionic strength of marine medium also led to lower Ni/Fe ratios in ferrihydrite precipitated in the marine medium compared to the Ni/Fe ratios in ferrihydrite precipitated in freshwater medium. In the marine medium, other divalent cations present in high abundance, such as Mg^{2+} and Ca^{2+}, but also anions such as HCO_3^-, will compete with the Ni and reduce the ability of Ni to bind to the surface of ferrihydrite.

The most interesting difference in Ni sorption and Ni co-precipitation was observed for biogenic compared to abiogenic ferrihydrite. While the concentration of sorbed or co-precipitated Ni is slightly higher for biogenic as compared to abiogenic ferrihydrite when normalized to the respective SSA (Table S5), the overall observed Ni sorption (and co-precipitation as a mechanism including sorption) is lower for biogenic ferrihydrite when looking at the molar Ni/Fe ratios (Fig. 3). This is in agreement with the higher crystallinity of biogenic ferrihydrite as observed by Mössbauer spectroscopy, and is also consistent with the higher SSA of abiogenic ferrihydrite. However, as discussed in Section 4.1, results of BET measurements of biogenic ferrihydrite have to be regarded with care as vacuum drying might lead to artefacts with organics or cells blocking sorption sites and micropores, thereby distorting the actual SSA of the mineral.

Regardless of the accuracy of the SSA, microbially-derived organics or whole cells in biogenic ferrihydrite bind to the mineral surface and compete with the Ni for sorption sites, explaining the lower sorption of Ni to biogenic ferrihydrite. Additionally, as shown by STXM, in the biogenic ferrihydrite (consisting of cell-Fe(III) mineral aggregates) Ni was co-localized with Fe, but not with the bacterial cells or other organic substances. This is in agreement with a study of an environmental biofilm, in which Ni was associated with the Fe-encrusted sheaths of filamentous bacteria, but not with bacterial cells that were unmineralized (Hitchcock et al., 2009).

The question is why does Ni preferably sorb to ferrihydrite mineral surfaces and not to the microbial cell surfaces? Metal sorption to cells or to Fe(III) (oxyhydr)oxides is based on proton exchange reactions. The proton-active sites on the cell wall of Gram-negative anoxygenic phototrophs are carboxyl, phosphoryl, phosphodiester and amine moieties (Pokrovsky et al., 2013), of which the carboxyl and phosphoryl moieties are deprotonated at neutral pH, as present in our experiments. In a previous study applying surface complexation modeling using a Linear Programming Model approach (LPM) described by Martinez et al. (2004), Pokrovsky et al. (2013) determined binding constants for Ni adsorption to the cell wall of an anoxygenic phototroph with pK values of -1.45 ± 0.05, 0.35 ± 0.05 and 5.0 with site densities of 0.418, 0.34 and 0.0287 µmol/g wet biomass, respectively (Pokrovsky et al., 2013). In comparison, pK values of -3.25 to 2.50 have been determined by surface complexation modeling for Ni sorption to hydrous ferric oxide with a confidence level of 0.99 and a total binding site density of 0.2 mol/mol for weak and 0.005 mol/mol for strong binding sites (corresponding to 2222 and 55.5 µmol/g HFO, respectively (Dzombak and Morel, 1990)). The lower pK values for Ni sorption to HFO and the higher binding site density on the mineral surface as compared to the cell wall allow a higher affinity of Ni for HFO and can explain the preferential sorption of Ni to ferrihydrite in cell–mineral aggregates in the present study. It has to be kept in mind, however, that their experiments were performed with washed cell or mineral suspensions in a $NaNO_3$ electrolyte and the values are not directly comparable to our studies in which media containing other potentially interfering ions were used.

Extended X-ray absorption fine structure (EXAFS) studies of Ni sorption to Fe(III) (oxyhxydr)oxides have

shown that Ni mostly forms edge-sharing surface complexes with inner-sphere mononuclear bidentate coordination (Xu et al., 2007; Arai, 2008). Corner-sharing surface complexes with inner-sphere mononuclear monodentate coordination have also been detected in minor abundance (Arai, 2008). While EXAFS studies on biogenic cell–Fe(III) mineral aggregates have not yet been performed, EXAFS data of Ni sorption by biomass–birnessite assemblages at pH 7 led to estimations of fractional contributions of Ni sorption to birnessite (0.30), Ni sorption to biomass (0.45) and Ni precipitation as $Ni(OH)_2$ (0.23) by linear combination fitting (Peña et al., 2011). Those authors concluded that biomass does not block reactive surface sites on the mineral, but that it contributes to Ni sorption at high metal loading when high-affinity sites on the mineral surface are saturated or unavailable. It should be noted that the Ni/sorbent ratio used in their study was ten times higher than in our study and moreover, the Mn(II)-oxidizing bacterium *Pseudomonas putida* was grown in a nutrient-rich medium, likely to much higher cell densities than the photoferrotrophs in our study. The higher Ni loadings and higher contribution of cell surfaces to the overall available reactive surface sites could be a possible explanation for their observation that biomass contributed to Ni sorption, which is in contrast to our observations where the Ni was mostly associated with the Fe minerals and not the biomass. A blocking of reactive mineral surface sites by microbial cells and their organic compounds in combination with lower Ni affinity to the cell surface sites as compared to Fe(III) (oxyhydr)oxide mineral surface sites best explains our observations.

4.3. Influence of Si on Ni partitioning in biogenic versus abiogenic ferrihydrite

In most experiments, the presence of Si during ferrihydrite precipitation did not significantly influence Ni sorption or co-precipitation with ferrihydrite on a quantitative basis, although local heterogeneities were observed. This is in contrast to previous studies in which Ni showed attenuated sorption to ferrihydrite by one order of magnitude in the presence of Si due to Si competing for sorption sites (Konhauser et al., 2009). These differences can potentially be explained by the applied Si/Fe ratios; the previous study used a Si/Fe ratio of 12:1 (Konhauser et al., 2007, 2009) which is representative for the Archean ocean (0.02–0.5 mM Fe; Holland, 1973; Morris, 1993; 2.2 mM Si; Maliva et al., 2005), while a higher Fe concentration (2 mM) was used in our study to ensure microbial growth necessary for visualization of cells by STXM, yielding a Si/Fe ratio of 1:1. Indeed, the spatial distribution of Fe, Si and Ni analyzed by STXM showed a co-localization of Fe and Si, confirming the potential blocking of Fe mineral sorption sites for Ni by Si, as might be expected at the much lower Fe concentrations of the Archean oceans. Therefore, the higher Fe content in our experiments provided sufficient surface area and thus sorption sites for both Ni and Si, so that the Si did not influence Ni sorption. This is supported by a previous report demonstrating that at a concentration of 2 mM Fe, the role of 2 mM Si for phosphate sorption to

ferrihydrite becomes negligible (Konhauser et al., 2007), which seems to be consistent with our findings. Moreover, as mentioned above, this study used Ni/Fe ratios 4× higher than in the study by Konhauser et al. (2009), leading to Ni/Fe ratios in the solid products above 0.01 versus 0.0025 for Si-rich particles in Konhauser et al. (2009). Accordingly, our use of higher Ni concentrations here facilitated greater Ni sorption. However, sorption isotherms indicate that an increase of the Ni/Fe ratio by a factor of 4 at these high Ni concentrations leads to an increase of the amount of adsorbed Ni by approximately a factor of 2–2.5 (Fig. S3).

Despite the negligible effect of Si on dissolved Ni concentrations in our experiments here, STXM analyses did reveal effects of Si at a small-scale in biogenic ferrihydrite. These samples showed heterogeneities with respect to cell encrustation, with some cells being encrusted in a mineral containing Fe and Si, while others were not encrusted at all. It has been shown before that phototrophic Fe(II)-oxidizers do not, or at least not to a large extent, encrust in the Fe(III) (oxyhydr)oxide minerals they precipitate (Kappler and Newman, 2004; Jiao et al., 2005; Miot et al., 2009b; Schädler et al., 2009; Hegler et al., 2010; Posth et al., 2010). This is due to an acidic microenvironment around the cell that prevents Fe(III) mineral precipitation on their cell wall, probably in combination with the excretion of EPS that function as nucleation centers distal to the cells (Kappler and Newman, 2004; Schädler et al., 2009; Hegler et al., 2010; Saraiva et al., 2012). This raises the questions of why and how do some of the cells get encrusted in our experiments, whether the Si binds directly to the cell surface or to ferrihydrite encrusting the cells, and whether Fe–Si minerals are formed? In previous studies of an environmental biofilm, Si was co-located with the Fe-rich sheaths of filamentous bacteria, but was interpreted as organosilicate based on spectroscopic C–O–Si bond signals (Hitchcock et al., 2009). While direct Si binding to cell surface sites has been demonstrated in lab experiments (Urrutia and Beveridge, 1993; Toporski et al., 2002), environmental samples from hot springs, hydrothermal vents and freshwater biofilms showed that an initial binding of Fe cations to anionic cell surface sites, followed by Fe mineral precipitation and reaction of $Si(OH)_4$ with Fe mineral surface hydroxyl groups (Juniper and Fouquet, 1988; Konhauser et al., 1993, 1994, 1998; Konhauser and Ferris, 1996) or sorption of Si to Fe-rich microbial sheaths (Köhler et al., 1994), facilitates silica sorption. In other words, Fe acts as a cation bridge for silica precipitation on microbial surfaces (Phoenix et al., 2003). In our experiments, the increased quadrupole splitting observed in Mössbauer spectra of biogenic ferrihydrite precipitated in the presence of Si indicates the incorporation of Si into the crystal lattice of ferrihydrite. This suggests the encrustation of the cells by a Fe–Si co-precipitate (siliceous ferrihydrite). As metabolically active phototrophic Fe(II)-oxidizing bacteria were shown not to encrust, and since we observed only a few encrusted cells, we believe that a small fraction of dead cells in our cultures were not able to actively maintain their acidic microenvironment, thereby facilitating mineral precipitation on the cell wall. This is consistent with other studies that have shown live,

dormant, moribund and dead cells differing in their mineralization behavior (Urrutia et al., 1992; Toporski et al., 2002). In support of this, dead cells show an increased availability of functional groups capable of metal binding as a result of cellular degradation (Ferris et al., 1988).

4.4. Implications for ancient environments

BIFs preserve an archive of early ocean chemistry due to the scavenging of trace metals by the precipitating Fe(III) (oxyhydr)oxides during the oxidation of dissolved Fe(II). Experimentally-derived partition coefficients of these trace metals and comparison to trace metal concentrations in BIFs have been used to estimate their dissolved concentration and bioavailability in the early ocean. This allows us to draw conclusions regarding microbial activity and the evolution of the biosphere at the time of mineral deposition based on trace metal requirements of modern organisms (Bjerrum and Canfield, 2002; Konhauser et al., 2007, 2009; Robbins et al., 2013). One study suggested that phosphate sorption onto Fe(III) (oxyhydr)oxides would have led to phosphate limitation and reduced oxygen production by phototrophic organisms, resulting in a delay in atmospheric oxygenation during the late Archean (Bjerrum and Canfield, 2002). This theory was challenged by experiments considering elevated Si concentrations (2.2 mM; Maliva et al., 2005), consistent with the lack of a biological Si removal in early oceans, that showed that Si would have out-competed phosphate for binding to Fe(III) (oxyhydr)oxides, rendering the so-called "Archean phosphate crisis" unlikely (Konhauser et al., 2007; Planavsky et al., 2010b). Subsequent studies estimated Archean ocean Ni and Zn concentrations based on partitioning of these elements in Fe(III) (oxyhydr)oxides in the presence of Si (Konhauser et al., 2009; Robbins, 2013). However, all these studies used chemically synthesized Fe(III) (oxyhydr)oxides as a proxy for naturally occurring Fe minerals, despite the potential for a biogenic origin of primary minerals in BIFs (e.g., Widdel et al., 1993; Konhauser et al., 2002; Kappler et al., 2005; Johnson et al., 2008; Posth et al., 2008; Planavsky et al., 2010a).

Biogenic Fe(III) (oxyhydr)oxide minerals differ from abiogenic minerals due to the presence of microbially-derived organic material (e.g. Ferris, 2005; Posth et al., 2010), and in the present study, we demonstrated that abiogenic ferrihydrite sorbed and co-precipitated more Ni than biogenic ferrihydrite. A previous study that used chemically synthesized Fe(III) (oxyhydr)oxides as proxies for primary BIF minerals calculated Ni concentrations in the Archean ocean to have dropped from 400 nM to below 200 nM by 2.5 Ga ago (Konhauser et al., 2009), thereby limiting methanogen activity since several enzymes in methanogens require Ni as a co-factor. Observations that Ni concentrations below 100 nM lead to reduced methanogen cell numbers (Schönheit et al., 1979) and methane production decreased at 250 nM Ni (Kida et al., 2001) agree with a potential methanogen famine when Ni concentrations dropped to 200 nM at the end of the Archean. Taking into account our data that showed that Ni sorption to biogenic ferrihydrite was two to three times lower than to abiogenic

minerals, and assuming a biogenic origin for at least a part of the primary BIF minerals, it is possible that the Ni concentration in the Archean oceans may have been even higher than previously thought. This has two implications. First, it supports the premise that the Archean oceans could have supported an extensive methanogen community, not only in the bottom sediments, but presumably throughout much of the water column. Indeed, the ^{13}C content of preserved organic carbon in various sedimentary lithologies ca. 2.70 Ga has been used to argue for methane-dominated ecosystems in both shallow- and deep-water environments at that time (Eigenbrode and Freeman, 2006). Second, Konhauser et al. (2009) proposed that dissolved Ni concentrations dropped below a critical threshold for methanogens in the water column shortly after 2.7 Ga, but if marine Ni concentrations were actually higher than initially assumed, then the methanogen famine could have been delayed to just prior the Great Oxidation Event at ca. 2.45 Ga (Konhauser et al., 2011b). This implies that the progression from an anoxic to oxic water column, and ultimately the transition from an anoxic to oxic atmosphere, might have taken place within tens of millions of years.

However, comparing the data of our study to those presented by Konhauser et al. (2009) requires caution. While Konhauser et al. (2009) used concentrations of Ni (0–4000 nM) and Fe (0.179 mM) believed to be representative for the Archean ocean (Ni: 400 nM, Konhauser et al., 2009; Fe: 0.02–0.5 mM, Holland, 1973; Morris, 1993), the concentrations used in our study were constrained by experimental limitations: a concentration of 2 mM Fe(II) was used for microbial Fe(II) oxidation to grow enough cells for a visualization with STXM, and 10 mg/L (170 μM) Ni were required to be above the quantification limit for STXM analysis (Hitchcock et al., 2009). Using these particular concentrations (especially Fe concentration) excludes a Si/Fe ratio relevant for the Archean ocean and does not allow drawing direct conclusions on the effects of Si on the partitioning of Ni in ferrihydrite in ancient environments.

5. CONCLUSIONS

Our experiments have demonstrated that the sorption and co-precipitation of Ni with ferrihydrite are reduced by the presence of microbially-derived organics and by ions present in marine medium. Silica co-precipitated with the ferrihydrite, but did not quantitatively influence the amount of Ni sorbed or co-precipitated at the Fe, Ni and Si concentrations tested. Since naturally occurring Fe(III) (oxyhydr)oxides contain similar impurities (e.g., Cismasu et al., 2011), considering organic material and interfering ions in experimental model systems is critical for a better understanding of the availability and fate of trace metals in modern and ancient natural environments. To obtain a full picture of the fate and bioavailability of trace metals in ancient oceans, however, remobilization processes such as microbial (Zachara et al., 2001; Crowe et al., 2007) and abiotic (diagenetic) mineral transformation processes (e.g., Frierdich et al., 2011; Köhler et al., 2013; Posth et al., 2013a; Robbins, 2013) have to be considered as well.

APPENDIX A. SUPPLEMENTARY DATA

Supplementary data associated with this article can be found, in the online version, at http://dx.doi.org/10.1016/j.gca.2014.05.021.

REFERENCES

Anbar A. D. (2008) Elements and evolution. *Science* **322**, 1481–1483.

Arai Y. (2008) Spectroscopic evidence for Ni(II) surface speciation at the iron oxyhydroxides−water interface. *Environ. Sci. Technol.* **42**, 1151–1156.

Bearden J. A. and Burr A. F. (1967) Reevaluation of X-ray atomic energy levels. *Rev. Mod. Phys.* **39**, 125–142.

Bjerrum C. J. and Canfield D. E. (2002) Ocean productivity before about 1.9 Gyr ago limited by phosphorus adsorption onto iron oxides. *Nature* **417**, 159–162.

Bluhm H., Andersson K., Araki T., Benzerara K., Brown G. E., Dynes J. J., Ghosal S., Gilles M. K., Hansen H. C., Hemminger J. C., Hitchcock A. P., Ketteler G., Kilcoyne A. L. D., Kneedler E., Lawrence J. R., Leppard G. G., Majzlan J., Mun B. S., Myneni S. C. B., Nilsson A., Ogasawara H., Ogletree D. F., Pecher K., Salmeron M., Shuh D. K., Tonner B., Tyliszczak T., Warwick T. and Yoon T. H. (2006) Soft X-ray microscopy and spectroscopy at the molecular environmental science beamline at the Advanced Light Source. *J. Electron Spectrosc. Relat. Phenom.* **150**, 86–104.

Brown G. E., Henrich V. E., Casey W. H., Clark D. L., Eggleston C., Felmy A., Goodman D. W., Grätzel M., Maciel G., McCarthy M. I., Nealson K. H., Sverjensky D. A., Toney M. F. and Zachara J. M. (1998) Metal oxide surfaces and their interactions with aqueous solutions and microbial organisms. *Chem. Rev.* **99**, 77–174.

Chakarova K., Rusanov V. and Trautwein A. X. (2013) Study of deep sea Fe–Mn sediments and the possibility to use these formations as paleoclimatic indicator. *J. Atmos. Sol.-Terr. Phy.* **99**, 143–149.

Chi Fru E., Ivarsson M., Kilias S. P., Bengtson S., Belivanova V., Marone F., Fortin D., Broman C. and Stampanoni M. (2013) Fossilized iron bacteria reveal a pathway to the biological origin of banded iron formation. *Nat. Commun.* **4**.

Cismasu A. C., Michel F. M., Tcaciuc A. P., Tyliszczak T. and Brown, Jr., G. E. (2011) Composition and structural aspects of naturally occurring ferrihydrite. *C. R. Geosci.* **343**, 210–218.

Clarke W. A., Konhauser K. O., Thomas J. C. and Bottrell S. H. (1997) Ferric hydroxide and ferric hydroxysulfate precipitation by bacteria in an acid mine drainage lagoon. *FEMS Microbiol. Rev.* **20**, 351–361.

Cornell R. and Schwertmann U. (2003) *The Iron Oxides: Structures, Properties, Reactions, Occurrences and Uses*, 2 ed. Wiley-VCH, Weinheim.

Crowe S. A., O'Neill A. H., Weisener C. G., Kulczycki E., Fowle D. A. and Roberts J. A. (2007) Reductive dissolution of trace metals from sediments. *Geomicrobiol. J.* **24**, 157–165.

Doelsch E., Rose J., Masion A., Bottero J. Y., Nahon D. and Bertsch P. M. (2000) Speciation and crystal chemistry of iron(III) chloride hydrolyzed in the presence of SiO_4 ligands. 1. An FeK-edge EXAFS study. *Langmuir* **16**, 4726–4731.

Dynes J. J., Tyliszczak T., Araki T., Lawrence J. R., Swerhone G. D. W., Leppard G. G. and Hitchcock A. P. (2006) Speciation and quantitative mapping of metal species in microbial biofilms using scanning transmission X-ray microscopy. *Environ. Sci. Technol.* **40**, 1556–1565.

Dzombak D. A. and Morel F. M. M. (1990) *Surface Complexation Modeling: Hydrous Ferric Oxide*. Wiley, New York.

Eaton A. D., Clesceri L. S., Rice E. W. and Greenberg A. E. (2005) *Standard Methods for the Examination of Water and Wastewater*, 21st ed. American Public Health Association, Washington, DC.

Ehrenreich A. and Widdel F. (1994) Anaerobic oxidation of ferrous iron by purple bacteria, a new type of phototrophic metabolism. *Appl. Environ. Microbiol.* **60**, 4517–4526.

Eigenbrode J. L. and Freeman K. H. (2006) Late Archean rise of aerobic microbial ecosystems. *Proc. Natl. Acad. Sci. U.S.A.* **103**, 15759–15764.

Eusterhues K., Wagner F. E., Häusler W., Hanzlik M., Knicker H., Totsche K. U., Kögel-Knabner I. and Schwertmann U. (2008) Characterization of ferrihydrite-soil organic matter coprecipitates by X-ray diffraction and Mössbauer spectroscopy. *Environ. Sci. Technol.* **42**, 7891–7897.

Ferris F. G. (2005) Biogeochemical properties of bacteriogenic iron oxides. *Geomicrobiol. J.* **22**, 79–85.

Ferris F. G., Fyfe W. S. and Beveridge T. J. (1988) Metallic ion binding by *Bacillus subtilis*: implications for the fossilization of microorganisms. *Geology* **16**, 149–152.

Frierdich A. J., Luo Y. and Catalano J. G. (2011) Trace element cycling through iron oxide minerals during redox-driven dynamic recrystallization. *Geology* **39**, 1083–1086.

Hegler F., Posth N. R., Jiang J. and Kappler A. (2008) Physiology of phototrophic iron(II)-oxidizing bacteria-implications for modern and ancient environments. *FEMS Microbiol. Ecol.* **66**, 250–260.

Hegler F., Schmidt C., Schwarz H. and Kappler A. (2010) Does a low-pH microenvironment around phototrophic Fe^{II}-oxidizing bacteria prevent cell encrustation by Fe^{III} minerals? *FEMS Microbiol. Ecol.* **74**, 592–600.

Hitchcock, A. P. (2013) aXis2000 is written in Interactive Data Language (IDL) and available free for non-commercial use from <http://unicorn.mcmaster.ca/aXis2000.html>.

Hitchcock A. P., Dynes J. J., Lawrence J. R., Obst M., Swerhone G. D. W., Korber D. R. and Leppard G. G. (2009) Soft X-ray spectromicroscopy of nickel sorption in a natural river biofilm. *Geobiology* **7**, 432–453.

Holland H. D. (1973) The oceans: a possible source of iron in iron-formations. *Econ. Geol.* **68**, 1169–1172.

Jiao Y. Y. Q., Kappler A., Croal L. R. and Newman D. K. (2005) Isolation and characterization of a genetically tractable photoautotrophic Fe(II)-oxidizing bacterium, *Rhodopseudomonas palustris* strain TIE-1. *Appl. Environ. Microbiol.* **71**, 4487–4496.

Johnson C., Beard B. L., Klein C., Beukes N. J. and Roden E. E. (2008) Iron isotopes constrain biologic and abiologic processes in banded iron formation genesis. *Geochim. Cosmochim. Acta* **72**, 151–169.

Juniper S. K. and Fouquet Y. (1988) Filamentous iron silica deposits from modern and ancient hydrothermal sites. *Can. Mineral.* **26**, 859–869.

Kappler A. and Newman D. K. (2004) Formation of Fe(III)-minerals by Fe(II)-oxidizing photoautotrophic bacteria. *Geochim. Cosmochim. Acta* **68**, 1217–1226.

Kappler A., Pasquero C., Konhauser K. O. and Newman D. K. (2005) Deposition of banded iron formations by anoxygenic phototrophic Fe(II)-oxidizing bacteria. *Geology* **33**, 865–868.

Kaznatcheev K. V., Karunakaran C., Lanke U. D., Urquhart S. G., Obst M. and Hitchcock A. P. (2007) Soft X-ray spectromicroscopy beamline at the CLS: commissioning results. *Nucl. Instrum. Methods Phys. Res. Sect. A* **582**, 96–99.

Kida K., Shigematsu T., Kijima J., Numaguchi M., Mochinaga Y., Abe N. and Morimura S. (2001) Influence of Ni^{2+} and Co^{2+} on methanogenic activity and the amounts of coenzymes involved in methanogenesis. *J. Biosci. Bioeng.* **91**, 590–595.

Köhler B., Singer A. and Stoffers P. (1994) Biogenic nontronite from marine white smoker chimneys. *Clays Clay Miner.* **42**, 689–701.

Köhler I., Konhauser K. O., Papineau D., Bekker A. and Kappler A. (2013) Biological carbon precursor to diagenetic siderite with spherical structures in iron formations. *Nat. Commun.* **4**, 1741.

Konhauser K. O. and Ferris F. G. (1996) Diversity of iron and silica precipitation by microbial mats hydrothermal waters, Iceland: implications for Precambrian iron formations. *Geology* **24**, 323–326.

Konhauser K. O., Fyfe W. S., Ferris F. G. and Beveridge T. J. (1993) Metal sorption and mineral precipitation by bacteria in two Amazonian river systems: Rio Solimoes and Rio Negro, Brazil. *Geology* **21**, 1103–1106.

Konhauser K. O., Schultzelam S., Ferris F. G., Fyfe W. S., Longstaffe F. J. and Beveridge T. J. (1994) Mineral precipitation by epilithic biofilms in the Speed River, Ontario, Canada. *Appl. Environ. Microbiol.* **60**, 549–553.

Konhauser K. O., Fisher Q. J., Fyfe W. S., Longstaffe F. J. and Powell M. A. (1998) Authigenic mineralization and detrital clay binding by freshwater biofilms: the Brahmani River, India. *Geomicrobiol. J.* **15**, 209–222.

Konhauser K. O., Hamade T., Raiswell R., Morris R. C., Ferris F. G., Southam G. and Canfield D. E. (2002) Could bacteria have formed the Precambrian banded iron formations? *Geology* **30**, 1079–1082.

Konhauser K. O., Lalonde S. V., Amskold L. and Holland H. D. (2007) Was there really an Archean phosphate crisis? *Science* **315**, 1234–1234.

Konhauser K. O., Pecoits E., Lalonde S. V., Papineau D., Nisbet E. G., Barley M. E., Arndt N. T., Zahnle K. and Kamber B. S. (2009) Oceanic nickel depletion and a methanogen famine before the Great Oxidation Event. *Nature* **458**, 750–753.

Konhauser K. O., Kappler A. and Roden E. E. (2011a) Iron in microbial metabolisms. *Elements* **7**, 89–93.

Konhauser K. O., Lalonde S. V., Planavsky N. J., Pecoits E., Lyons T. W., Mojzsis S. J., Rouxel O. J., Barley M. E., Rosiere C., Fralick P. W., Kump L. R. and Bekker A. (2011b) Aerobic bacterial pyrite oxidation and acid rock drainage during the Great Oxidation Event. *Nature* **478**, 369–373.

Larese-Casanova P., Haderlein S. B. and Kappler A. (2010) Biomineralization of lepidocrocite and goethite by nitrate-reducing Fe(II)-oxidizing bacteria: effect of pH, bicarbonate, phosphate, and humic acids. *Geochim. Cosmochim. Acta* **74**, 3721–3734.

Maliva R. G., Knoll A. H. and Simonson B. M. (2005) Secular change in the Precambrian silica cycle: insights from chert petrology. *Geol. Soc. Am. Bull.* **117**, 835–845.

Martinez R. E., Pedersen K. and Ferris F. G. (2004) Cadmium complexation by bacteriogenic iron oxides from a subterranean environment. *J. Colloid Interface Sci.* **275**, 82–89.

Mikutta C., Mikutta R., Bonneville S., Wagner F., Voegelin A., Christl I. and Kretzschmar R. (2008) Synthetic coprecipitates of exopolysaccharides and ferrihydrite. Part I: Characterization. *Geochim. Cosmochim. Acta* **72**, 1111–1127.

Miot J., Benzerara K., Morin G., Kappler A., Bernard S., Obst M., Ferard C., Skouri-Panet F., Guigner J. M., Posth N., Galvez M., Brown G. E. and Guyot F. (2009a) Iron biomineralization by anaerobic neutrophilic iron-oxidizing bacteria. *Geochim. Cosmochim. Acta* **73**, 696–711.

Miot J., Benzerara K., Obst M., Kappler A., Hegler F., Schädler S., Bouchez C., Guyot F. and Morin G. (2009b) Extracellular iron biomineralization by photoautotrophic iron-oxidizing bacteria. *Appl. Environ. Microbiol.* **75**, 5586–5591.

Morris R. C. (1993) Genetic modelling for banded iron-formation of the Hamersley Group, Pilbara Craton, Western Australia. *Precambrian Res.* **60**, 243–286.

Muehe M., Scheer L., Daus B. and Kappler A. (2013) Fate of arsenic during microbial reduction of biogenic vs. abiogenic As–Fe(III)–mineral co-precipitates. *Environ. Sci. Technol.* **47**, 8297–8307.

Mulrooney S. B. and Hausinger R. P. (2003) Nickel uptake and utilization by microorganisms. *FEMS Microbiol. Rev.* **27**, 239–261.

Murad E. and Cashion J. J. (2004) *Mössbauer Spectroscopy of Environmental Materials and their Industrial Utilization*. Kluwer Academic Publishers.

Pantke C., Obst M., Benzerara K., Morin G., Ona-Nguema G., Dippon U. and Kappler A. (2011) Green rust formation during Fe(II) oxidation by the nitrate-reducing *Acidovorax* sp. strain BoFeN1. *Environ. Sci. Technol.* **46**, 1439–1446.

Parmar N., Gorby Y. A., Beveridge T. J. and Ferris F. G. (2001) Formation of green rust and immobilization of nickel in response to bacterial reduction of hydrous ferric oxide. *Geomicrobiol. J.* **18**, 375–385.

Peña J., Bargar J. and Sposito G. (2011) Role of bacterial biomass in the sorption of Ni by biomass–birnessite assemblages. *Environ. Sci. Technol.*, 7338–7344.

Pfennig N. (1978) *Rhodocyclus purpureus* gen. nov. and sp. nov., a ring-shaped, vitamin B_{12}-requiring member of the family *Rhodospirillaceae. Int. J. Syst. Bacteriol.* **28**, 283–288.

Phoenix V. R., Konhauser K. O. and Ferris F. G. (2003) Experimental study of iron and silica immobilization by bacteria in mixed Fe–Si systems: implications for microbial silicification in hot springs. *Can. J. Earth Sci.* **40**, 1669–1678.

Planavsky N., Rouxel O., Bekker A., Shapiro R., Fralick P. and Knudsen A. (2009) Iron-oxidizing microbial ecosystems thrived in late Paleoproterozoic redox-stratified oceans. *Earth Planet. Sci. Lett.* **286**, 230–242.

Planavsky N., Bekker A., Rouxel O. J., Kamber B., Hofmann A., Knudsen A. and Lyons T. W. (2010a) Rare Earth Element and yttrium compositions of Archean and Paleoproterozoic Fe formations revisited: new perspectives on the significance and mechanisms of deposition. *Geochim. Cosmochim. Acta* **74**, 6387–6405.

Planavsky N. J., Rouxel O. J., Bekker A., Lalonde S. V., Konhauser K. O., Reinhard C. T. and Lyons T. W. (2010b) The evolution of the marine phosphate reservoir. *Nature* **467**, 1088–1090.

Pokrovski G. S., Schott J., Garges F. and Hazemann J. L. (2003) Iron (III)–silica interactions in aqueous solution: insights from X-ray absorption fine structure spectroscopy. *Geochim. Cosmochim. Acta* **67**, 3559–3573.

Pokrovsky O. S., Martinez R. E., Kompantseva E. I. and Shirokova L. S. (2013) Interaction of metals and protons with anoxygenic phototrophic bacteria *Rhodobacter blasticus*. *Chem. Geol.* **335**, 75–86.

Posth N. R., Hegler F., Konhauser K. O. and Kappler A. (2008) Alternating Si and Fe deposition caused by temperature fluctuations in Precambrian oceans. *Nat. Geosci.* **1**, 703–708.

Posth N. R., Huelin S., Konhauser K. O. and Kappler A. (2010) Size, density and composition of cell–mineral aggregates formed during anoxygenic phototrophic Fe(II) oxidation: impact on modern and ancient environments. *Geochim. Cosmochim. Acta* **74**, 3476–3493.

Posth N. R., Köhler I., Swanner E. D., Schröder C., Wellmann E., Binder B., Konhauser K. O., Neumann U., Berthold C., Nowak M. and Kappler A. (2013a) Simulating Precambrian banded iron formation diagenesis. *Chem. Geol.* **362**, 66–73.

Posth N. R., Konhauser K. O. and Kappler A. (2013b) Microbiological processes in banded iron formation deposition. *Sedimentology* **60**, 1733–1754.

Rancourt D. G., Fortin D., Pichler T., Thibault P.-J., Lamarche G., Morris R. V. and Mercier P. H. J. (2001) Mineralogy of a natural As-rich hydrous ferric oxide coprecipitate formed by mixing of hydrothermal fluid and seawater: implications regarding surface complexation and color banding in ferrihydrite deposits. *Am. Mineral.* **86**, 834–851.

Robbins, L. J. (2013) Zinc in Precambrian Iron Formations: The Record, Partitioning, Diagenetic Effects and Implications for Eukaryotic Metallome Evolution. M.Sc. Thesis. University of Alberta, Edmonton, AB.

Robbins L. J., Lalonde S. V., Saito M. A., Planavsky N. J., Mloszewska A. M., Pecoits E., Scott C., Dupont C. L., Kappler A. and Konhauser K. O. (2013) Authigenic iron oxide proxies for marine zinc over geological time and implications for eukaryotic metallome evolution. *Geobiology* **11**, 295–306.

Saito M. A., Sigman D. M. and Morel F. M. M. (2003) The bioinorganic chemistry of the ancient ocean: the co-evolution of cyanobacterial metal requirements and biogeochemical cycles at the Archean-Proterozoic boundary? *Inorg. Chim. Acta* **356**, 308–318.

Saraiva I. H., Newman D. K. and Louro R. O. (2012) Functional characterization of the FoxE iron oxidoreductase from the photoferrotroph *Rhodobacter ferrooxidans* SW2. *J. Biol. Chem.* **287**, 25541–25548.

Schädler S., Burkhardt C., Hegler F., Straub K. L., Miot J., Benzerara K. and Kappler A. (2009) Formation of cell-iron-mineral aggregates by phototrophic and nitrate-reducing anaerobic Fe(II)-oxidizing bacteria. *Geomicrobiol. J.* **26**, 93–103.

Schönheit P., Moll J. and Thauer R. K. (1979) Nickel, cobalt, and molybdenum requirement for growth of *Methanobacterium thermoautotrophicum*. *Arch. Microbiol.* **123**, 105–107.

Schwertmann U., Wagner F. and Knicker H. (2005) Ferrihydrite–humic associations: magnetic hyperfine interactions. *Soil Sci. Soc. Am. J.* **69**, 1009–1015.

Stookey L. L. (1970) Ferrozine – a new spectrophotometric reagent for iron. *Anal. Chem.* **42**, 779–781.

Straub K. L., Rainey F. A. and Widdel F. (1999) *Rhodovulum iodosum* sp. nov. and *Rhodovulum robiginosum* sp. nov., two new marine phototrophic ferrous-iron-oxidizing purple bacteria. *Int. J. Syst. Bacteriol.* **49**, 729–735.

Toporski J. K. W., Steele A., Westall F., Thomas-Keprta K. L. and McKay D. S. (2002) Winner of the 2001 Gerald A. Soffen Memorial Award - The simulated silicification of bacteria - New clues to the modes and timing of bacterial preservation and implications for the search for extraterrestrial microfossils. *Astrobiology* **2**, 1–26.

Tschech A. and Pfennig N. (1984) Growth yield increase linked to caffeate reduction in *Acetobacterium woodii*. *Arch. Microbiol.* **137**, 163–167.

Urrutia M. M. and Beveridge T. J. (1993) Mechanism of silicate binding to the bacterial cell wall in *Bacillus subtilis*. *J. Bacteriol.* **175**, 1936–1945.

Urrutia M. M., Kemper M., Doyle R. and Beveridge T. J. (1992) The membrane-induced proton motive force influences the metal binding ability of *Bacillus subtilis* cell walls. *Appl. Environ. Microbiol.* **58**, 3837–3844.

Weber K. A., Achenbach L. A. and Coates J. D. (2006) Microorganisms pumping iron: anaerobic microbial iron oxidation and reduction. *Nat. Rev. Microbiol.* **4**, 752–764.

Widdel F., Kohring G.-W. and Mayer F. (1983) Studies on dissimilatory sulfate-reducing bacteria that decompose fatty acids. *Arch. Microbiol.* **134**, 286–294.

Widdel F., Schnell S., Heising S., Ehrenreich A., Assmus B. and Schink B. (1993) Ferrous iron oxidation by anoxygenic phototrophic bacteria. *Nature* **362**, 834–836.

Xu Y., Axe L., Boonfueng T., Tyson T. A., Trivedi P. and Pandya K. (2007) Ni(II) complexation to amorphous hydrous ferric oxide: an X-ray absorption spectroscopy study. *J. Colloid Interface Sci.* **314**, 10–17.

Zachara J. M., Fredrickson J. K., Smith S. C. and Gassman P. L. (2001) Solubilization of Fe(III) oxide-bound trace metals by a dissimilatory Fe(III) reducing bacterium. *Geochim. Cosmochim. Acta* **65**, 75–93.

Zegeye A., Bonneville S., Benning L. G., Sturm A., Fowle D. A., Jones C., Canfield D. E., Ruby C., MacLean L. C., Nomosatryo S., Crowe S. A. and Poulton S. W. (2012) Green rust formation controls nutrient availability in a ferruginous water column. *Geology* **40**, 599–602.

Zerkle A. L., House C. H. and Brantley S. L. (2005) Biogeochemical signatures through time as inferred from whole microbial genomes. *Am. J. Sci.* **305**, 467–502.

Associate editor: Marc Norman